Experiments in Fluids 32 (2002) 580–589 © Springer-Verlag 2002
DOI 10.1007/s00348-001-0401-8

An experimental study of a water droplet impinging on a liquid surface

S. L. Manzello, J. C. Yang

Abstract An experimental study is presented for water droplet impingement on a liquid surface. The impaction process was recorded using a high-speed digital camera at 1,000 frames/s. The initial droplet diameter was fixed at 3.1 mm ± 0.1 mm, and all experiments were performed in atmospheric air. The impact velocity was varied from 0.36 m/s to 2.2 m/s thus varying the impact Weber number from 5.5 to 206. The impacted liquid surface consisted of two fluids, namely water and methoxy-nonafluorobutane, $C_4F_9OCH_3$ (HFE7100). The depth of the water and HFE7100 pool was varied from 2 mm to 25 mm. The collision dynamics of water in the HFE7100 pool was observed to be drastically different from that observed for the water droplet impingement on a water pool. The critical impact Weber number for jet breakup was found to be independent of liquid depth. Water–HFE7100 impact resulted in no jet breakup over the range of velocities studied. Therefore, no critical impact Weber number can be defined for water–HFE7100 impact.

1 Introduction

Liquid droplet interaction with a surface has been studied for more than 100 years (Reynolds 1875, 1881). Practical applications of a droplet colliding with a surface include spray cooling of turbine blades, electronic devices, and internal combustion engines. Droplet surface interaction is also important in agriculture, atmospheric sciences, criminal forensics, and fire suppression by sprinkler systems. The characteristics of the droplet/surface interactions depend upon the properties of the droplet, the impacted surface, impact velocity, geometry, and the medium (liquid, gas, dispersion) through which the droplet traverses prior to impact (Rein 1993). Despite many investigations, the complicated fluid mechanic processes associated with liquid droplet/surface interaction is not yet well understood (Rein 1993).

An important distinction made for liquid droplet/surface interaction is the type of impacted surface. The target surface can be either a solid or a liquid surface. Depending upon the type of surface, the collision dynamics of the impinging droplet can be vastly different (Rein 1993). The fluid mechanics of droplet collision with a solid surface has been studied in great detail (Engel 1955; Bowden and Field 1964; Levin and Hobbs 1971; Lesser 1981; Al-Durrah and Bradford 1982; Oliver 1984; Avedisian and Koplik 1987; Chandra and Avedisian 1991, 1992; Ko and Chung 1996; Bola and Chandra 1999; Aziz and Chandra 2000; Kang and Lee 2000). Droplet collision with liquid surfaces, however, has been studied in considerably less detail (Reynolds 1875, 1881; Thomson and Newall 1885; Worthington 1908; Schotland 1960; Jayaratne and Mason 1964; Macklin and Hobbs 1969; Rodriguez and Mesler 1985, 1988; Hsiao et al. 1988; Cai 1989; Pumphrey et al. 1989; Shin and McMahon, 1990; Zhbankova and Kolpakov 1990; Rein 1996; Wang and Chen 2000).

The impact of a liquid droplet with a liquid surface can result in droplet floating, bouncing, coalescing, and splashing on the liquid surface. Rodriguez and Mesler (1985) have delineated the processes of coalescence and splashing for water droplets impacting upon a water pool. In their experiments, the droplet impingement process was imaged using a high-speed motion picture camera at 1,000 frames/s. The droplet size and velocity were varied from 0.5 mm to 4.5 mm and 0.3 m/s to 2.4 m/s, respectively. Impacts that resulted in the formation of jets were termed splashes, and drops causing formation of vortex rings were defined as coalescing drops (Rodriguez and Mesler 1985). Rodriguez and Mesler (1985) generated a regime map dependent on the Froude number, $U/(gD)^{1/2}$, and Reynolds number, $DU\rho/\mu$, where g is the gravitational acceleration, U is the droplet impact velocity, D is the droplet diameter, ρ is the liquid density, and μ the liquid viscosity. For a Reynolds number larger than 3,000 and for a Froude number between 6 and 18, impact of a water droplet with a water pool will result in a splash (Rodriguez and Mesler 1985).

Rein (1996) extended the work of Rodriguez and Mesler (1985) by investigating the transition regime for coalescing and splashing drops. Water droplets impacted a water pool and the collision dynamics were imaged using a

Received: 27 June 2001/Accepted: 29 November 2001

S. L. Manzello (✉), J. C. Yang
Building and Fire Research Laboratory
National Institute of Standards and Technology
Gaithersburg, MD 20899, USA
e-mail: Samuel.Manzello@nist.gov

The authors wish to thank Dr. Rodney Bryant of NIST for providing the PC used for data acquisition. SLM acknowledges support from an NRC Post-Doctoral Fellowship.

high-speed camera with a framing rate of 500 frames/s. The droplet diameter and velocity were varied from 2.2 mm to 2.5 mm and 0.6 m/s to 2.6 m/s, respectively. The impact Weber number was defined as, $We = \rho U^2 D/\sigma$, where σ is the liquid surface tension. The impact Weber number was found to be the main parameter influencing the transition from coalescing to splashing (Rein 1996). The Froude number was found to influence transition but to a lesser degree than the Weber number (Rein 1996). Thus, a regime map was generated as a function of impacting Weber number. Rein (1996) observed that below a critical Weber number, coalescence of the impinging droplet resulted. As the Weber number was increased, a jet was observed to rise above the free surface. Rein (1996) further separated the jetting region into several sub-categories. At a Weber number just above the transition to jetting, a thick jet was observed to rise above the free surface with no secondary jet formation. Subsequent increase in Weber number resulted in thin high-rising jets with several tiny droplets ejected from the jet. These thin high-rising jets were observed to occur within the region of regular entrapment. The region of regular entrapment was previously classified as the region within Weber and Froude number space where a gas bubble is entrained within the liquid after impact (Pumphrey et al. 1989). Rein (1996) thus classified the region of regular entrapment as that region where a bubble is entrained within the liquid in conjunction with the presence of high rising jets. Increasing the Weber number yet further, beyond the region of regular entrapment, resulted in thick jets with large droplets breaking off from the jet. Numerical values of Weber number for the transition from one regime to another were not assigned, since the transitions did not occur exactly at a certain Weber number.

Whereas Rodriguez and Mesler (1985) and Rein (1996) focused upon liquid droplet impingement normal to the liquid surface, Zhbankova and Kolpakov (1990) generated a regime map as a function of impinging droplet angle. Water droplets were used, and the impacted surface was a water pool. A stream of drops was generated at an impact frequency of 40–60 Hz, thus it was assumed that the low-impact frequency allowed the liquid surface to recover during successive collisions. The droplet sizes were varied from 150 μm to 300 μm and the impact angle from of 16° to 85°. The impact Weber number, $We = U^2 r_1 \rho/\sigma$ was correlated with the type of impact versus the impinging droplet angle. The authors defined r_1 and V as the droplet radius and velocity at impact. The type of impact was found to be sensitive to the Weber number and the droplet collision angle.

Rodriguez and Mesler (1985), Zhbankova and Kolpakov (1990), and Rein (1996) made no reference to the depth of the liquid pool used in their experiments. Rather, it was assumed that the liquid pool was sufficiently deep and thus had no effect on the droplet collision process. The influence of liquid depth on collision dynamics was considered by Macklin and Hobbs (1969). Distilled water droplets were allowed to impact a distilled water pool. The droplet size and velocity were fixed at 2.3 mm and 3.2 m/s, respectively. The liquid depth was varied from 1 mm to 25 mm. The collision dynamics were imaged using a 16-mm high-speed camera with a framing rate of 480 frames/s. The number of jet fragments, maximum jet height, and the initial jet speed were measured as functions of liquid pool depth. It was observed that the maximum jet height increased with increasing depth and subsequently decreased as the liquid pool depth was increased beyond 7 mm. This phenomenon was believed to be due to the interaction of the cavity formed below the surface (from droplet impact) with the solid surface under the liquid.

Wang and Chen (2000) developed a novel technique for studying droplet impact on very thin films of fluid. The non-dimensional depth of the liquid surface was defined as H^*, where H^* was equal to the film thickness divided by the droplet diameter. The droplet diameter was varied from 4.2 mm to 4.6 mm and three different fluids were used: a 60% glycerol–water solution by weight; a 70% glycerol–water solution by weight; and an 80% glycerol–water solution by weight. H^* was varied from 0.05 to 0.1, thus varying the liquid depth from 0.23 mm to 0.46 mm. The critical impact Weber number for splashing was determined as a function of the non-dimensional liquid depth. Splashing was defined as those impacts where secondary droplets were ejected from the crown upon impact. The critical impact Weber number for splashing was found to be independent of liquid depth. Impact with the 80% glycerol–water solution was found to have the highest critical impact Weber number for splashing, equal to 800. The 60% and 70% glycerol–water solution resulted in critical impact Weber numbers for splashing of 400 and 500, respectively. Differences in the critical impact Weber number for the different glycerol–water solutions were believed to be due to differences in the liquid viscosity.

Most experiments involving droplet interaction with a liquid surface have not investigated droplet impact upon liquids comprising a fluid different from that of the impinging droplet (Rein 1993). Thompson and Newall (1885) observed vortex ring formation in a variety of target fluids that were different from the impinging droplet. However, water–water impact is most often studied (Macklin and Hobbs 1969; Rodriguez and Mesler 1985; Zhbankova and Kolpakov 1990; Rein 1996). In addition, mercury–mercury (Hsaio et al. 1988) impact, methanol–water droplet impact with a methanol–water pool (Shin and McMahon 1990), and glycerol–water impact with a glycerol–water pool have been investigated (Wang and Chen 2000). Hence, the motivation for the present study was to examine droplet impingement on a liquid surface consisting of a fluid different from the impacting droplet. In particular, two targeting liquids with vast differences in their thermophysical properties were chosen in this work. Methoxynonafluorobutane, $C_4F_9OCH_3$ (HFE7100) was selected in the present study because it has a surface tension much

Table 1. Selected thermophysical properties of the target liquid

Fluid	Density (ρ) (kg/m^3)	Dynamic viscosity (μ) (Ns/m^2)	Surface tension (σ) (N/m)
H_2O at 25 °C	996.9	8.9×10^{-4}	0.072
HFE7100 at 25 °C	1,500	6.1×10^{-4}	0.0136

lower than water. At 25 °C, the surface tension of water is 0.072 N/m compared with that of 0.0136 N/m for HFE7100. Other physical properties of HFE7100 and water are listed in Table 1. This dynamic collision process was compared with droplet impingement with a liquid surface containing the same fluid as the impinging droplet. In addition to using two different fluids as targets, the effect of the depth of the liquid pool and droplet velocity on the dynamic collision process was also examined.

Comparing droplet collision dynamics with a low surface tension fluid was imperative, since the goal of the authors is to study droplet dynamics with a burning liquid surface from a fire-suppression perspective. Under these conditions, the liquid pool temperature at the surface is near the boiling point of the fluid. Such high temperatures will result in low surface tension of the pool at the surface. Thus, droplet collision dynamics were investigated using a non-burning low surface tension surrogate fluid (HFE7100) as a first step prior to experimenting with burning surfaces.

2
Experimental description

Figure 1 is a schematic of the experimental setup. The water droplets were generated using a syringe pump which was programmed to dispense the liquid at a rate of 0.001 mL/s. The droplet was formed at the tip of the needle and detached off the syringe under its own weight. To vary the droplet impact velocity, the height of the syringe pump above the liquid pool was varied (see Fig. 1). The container used to hold the liquid pool was a glass cylinder 90 mm in diameter. Since the droplet size for all experiments was fixed at 3.1 mm ± 0.1 mm (mean ± standard deviation), the diameter of the pool was 30 times larger than the initial droplet size. Thus, wall effects are not deemed important in the present study.

Droplet impingement was imaged using a Kodak Ekta-Pro 1000 HRC Digital High Speed Camera at 1000 frames/s with shutter speed set to 50 μs. The Kodak High Speed Camera was fitted with a Nikon 60-mm micro lens to obtain the required spatial resolution to capture droplet impingement. The entire process was back-lit using one 150-W light source (see Fig. 1). The impact velocity was measured by tracking the location of the droplet centroid 2 ms prior to impact using image-processing software. The image-processing software was also used to threshold the droplet from the background, and the diameter of the droplet was measured in both the horizontal and vertical directions. The difference in the diameter measured in both directions was at most 0.3 mm. Thus, the droplet diameter was defined as the average of these two measurements.

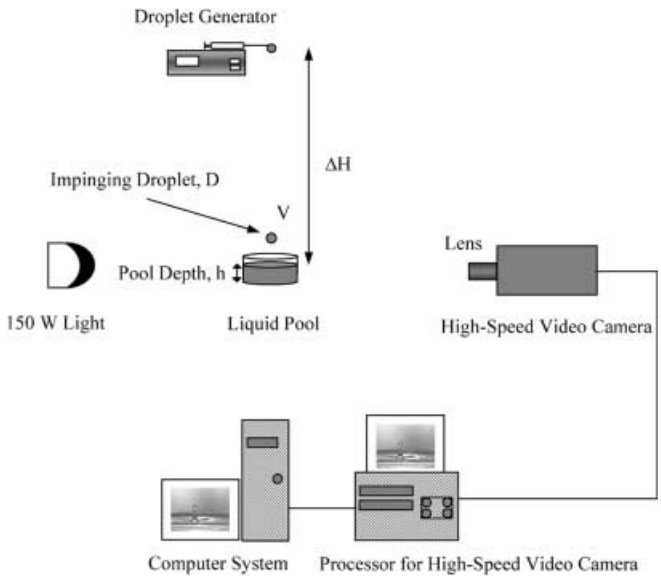

Fig. 1. Schematic of experimental setup

Distilled water was used to fill the syringe fitted in the syringe pump for droplet generation. One sequence of experiments was performed with distilled water used as the pool liquid. Another sequence of experiments was run with HFE7100 as the pool liquid. For both the water and HFE7100 pool, the liquid depth was varied from 2 mm to 25 mm.

3
Results and discussion

Several experiments were performed at each depth and velocity. The collision dynamics were repeatable for each case. Since each experiment displayed the same qualitative trends, the results of three consecutive experiments were used for data analysis. Figure 2 displays the time-elapsed images of water droplet impingement upon a 2-mm film of water and HFE7100 with an impact Weber number of 206. The impact Weber number in this study was defined as $We = \rho U^2 D/\sigma$, where D is the droplet diameter, U is the impact velocity, ρ is the droplet liquid density, and σ is the droplet liquid surface tension. The time in each sequence is defined as the time after droplet impact. Since the process beneath the surface was not the primary focus in the present study, the magnification of the lens was adjusted to give a field of view to record collision dynamics occurring above the liquid free surface and to capture the highest jet of fluid rising from the free surface before breakup. To facilitate comparison with different experimental conditions, all images were recorded using the same magnification. At a time of 6 ms after impact, the splash created by the water droplet in the 2-mm water layer (Fig. 2) resembles the classical crown shape photographed by Edgerton and Killian (1939). In the case of water droplet impact with the 2-mm HFE7100 pool (Fig. 2), however, no crown is observed to form. Rather, several droplets were immediately ejected from the surface upon impact. At 20 ms after impact, the collision dynamics have ended in the water pool, yet the process continued in the HFE7100 pool.

The next sequence considered is water droplets with impact $We = 206$ into a pool of 7-mm depth, also shown in Fig. 2. Water droplet impact into the water pool results in a splash with a jet (defined here as the column of liquid rising from the liquid surface) breaking up at a time of 55 ms after impact. For impact with HFE7100, at a time of 25 ms after impact, several droplets are ejected, as in the thin layer impact. At a time of 45 ms, a jet begins to rise

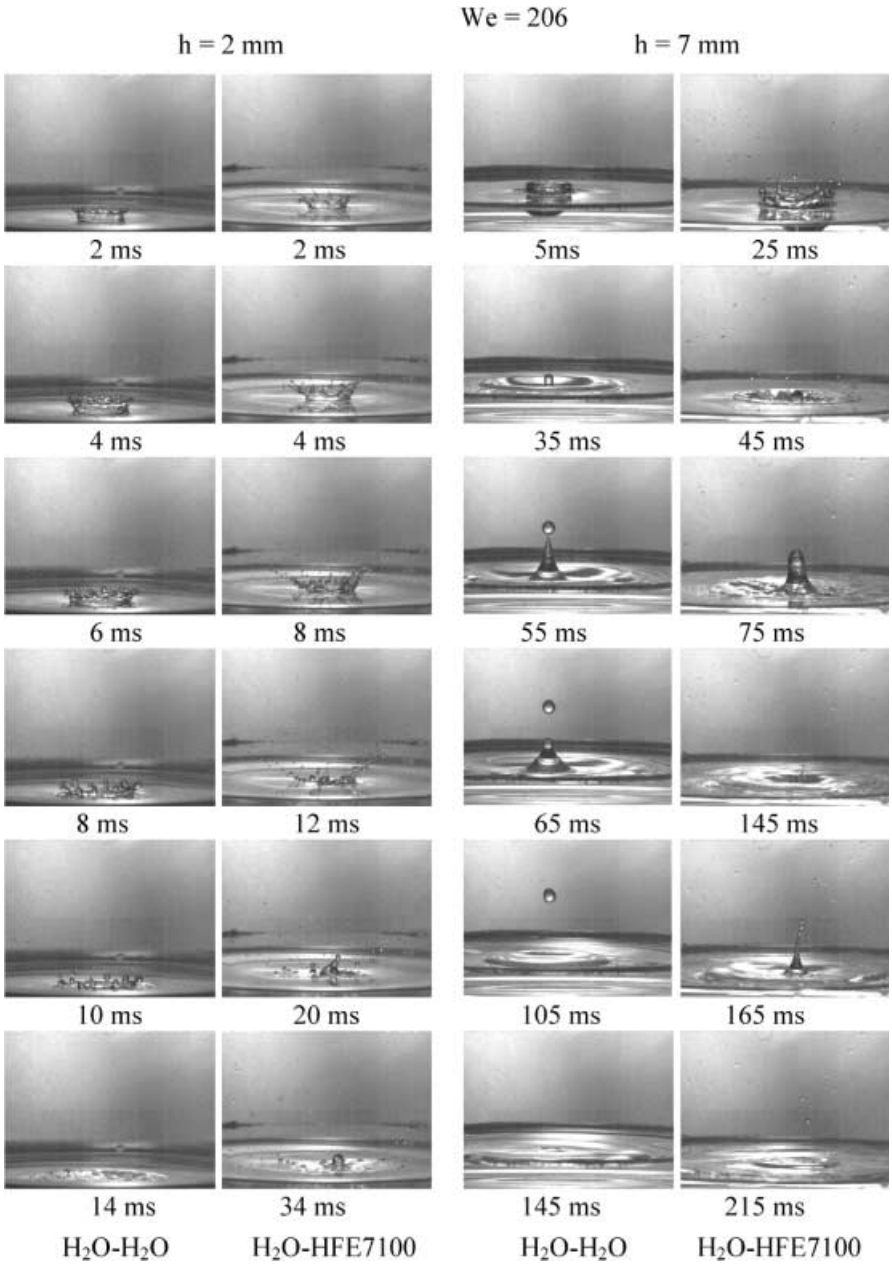

Fig. 2. Time-elapsed images of water droplet impingement upon a 2-mm and 7-mm liquid pool of water and HFE7100 for $We = 206$

from the pool and reaches a maximum height at 75 ms after impact. This jet does not break up, as in the water pool. Rather, it recedes back into the pool to create a secondary jet that begins to form at 145 ms after impact. Such behavior has been observed to occur by Worthington (1908) in water droplet impact with a liquid water pool from a height of 75 cm. The secondary jet subsequently breaks up into several small droplets, as seen at 165 ms after impact.

Increasing the depth to 10 mm for $We = 206$ (Fig. 3) results in jet breakup again for water–water impact. An interesting observation is that the droplets generated from the liquid jet float upon the liquid surface after returning to the surface. Such behavior has been observed by Rein (1996) for water–water impact. For water droplet impact with HFE7100, the resulting impact is similar to the case with a depth of 7 mm. At 41 ms, the jet begins to rise from the liquid. The jet reaches a maximum height at 75 ms and does not break up. It recedes into the pool and forms a secondary jet that breaks up, similar to the observation at a depth of 7 mm.

Figure 3 contains time-elapsed images for an increase in the pool depth to 25 mm for $We = 206$. At 25 mm, impact with the water pool forms a jet that is seen to break up at 35 ms after impact. Similar to the 10-mm depth, droplets generated from the liquid jet float upon the liquid surface after returning to the surface. For HFE7100 pool (Fig. 3), at a depth of 25 mm, few droplets are ejected from the surface upon initial impact. The small number of drops ejected at 25 mm for HFE7100 is different from the misting phenomenon observed for thinner depths, as seen in Figs. 2 and 3. Similar to the case of the 7-mm depth, at the 10-mm depth a jet is seen to rise from the surface after impact. However, after this jet recedes into the surface, no

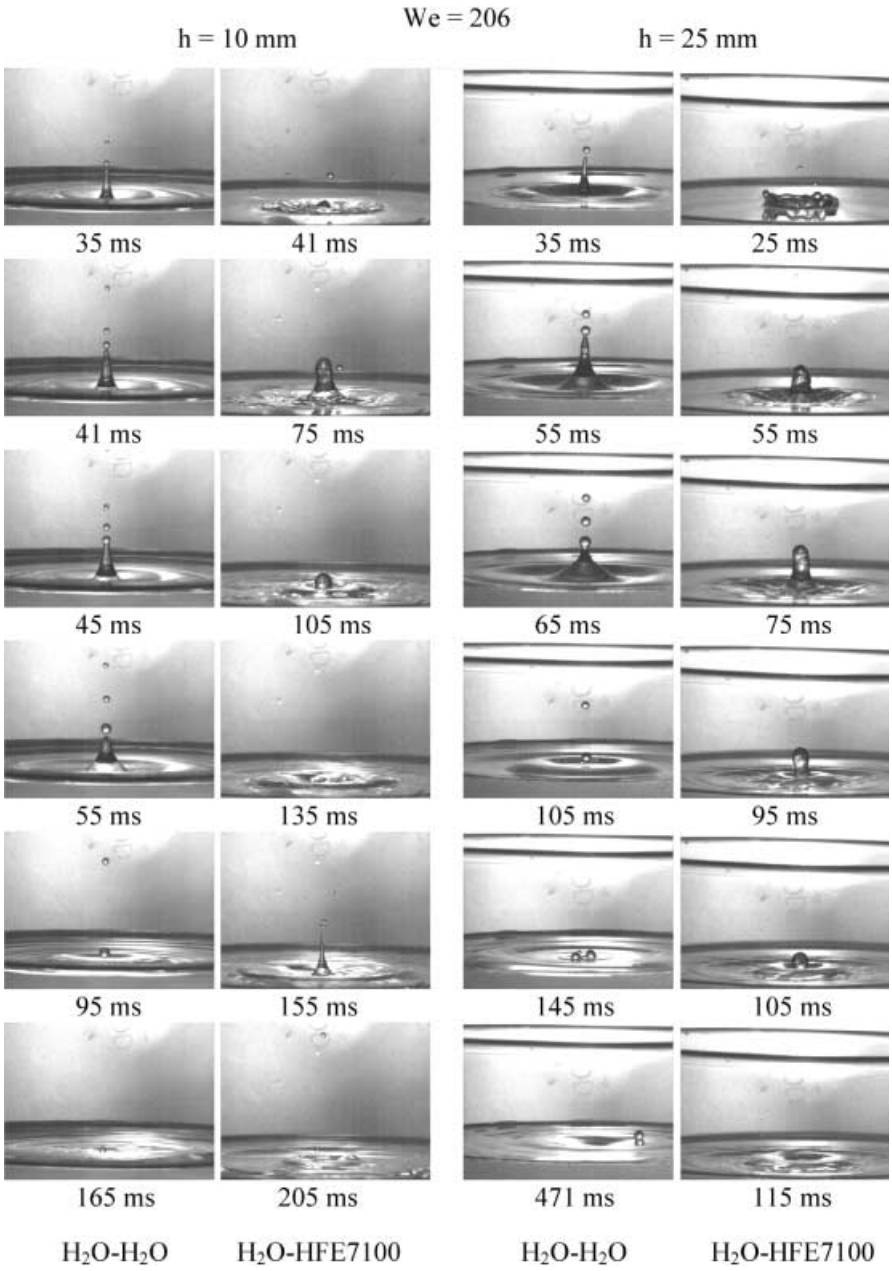

Fig. 3. Time-elapsed images of water droplet impingement upon a 10-mm and 25-mm liquid pool of water and HFE7100 for $We = 206$

secondary jet is observed to form as was observed at both 7-mm and 10-mm depths.

Figure 4 displays a sequence of images for water droplet impact upon a 2-mm depth pool of water and HFE7100 at $We = 123$. The effect of a reduction in impact velocity compared with $We = 206$ can be seen. The impact of the water droplet on the HFE7100 layer displays more symmetry compared with $We = 206$ (Fig. 3). The dramatic misting observed at $We = 206$ is not seen. For water–water impact, the formation of droplets emanating from the top of the crown (Fig. 4) does not occur. Rather, a crater is formed, and it quickly settles back into the pool.

Figures 4 and 5 display impact for $We = 123$ at 7-mm and 10-mm depths. For water–HFE7100 (Fig. 4) impact at 7-mm depth with $We = 123$, the initial phases of impact are similar to $We = 206$. At $We = 123$, however, after the jet recedes into the pool at 95 ms, no secondary jet forms as observed at the same depth with $We = 206$. For water–water impact (Fig. 4), the jet breaks up but the size of the ejected water droplet is much smaller than at $We = 206$. As the depth is increased to 10 mm for $We = 123$ (Fig. 5), impact of the water droplet into the HFE7100 pool results in secondary jet impact. The height of the secondary jet is lower than that obtained at the same depth at $We = 206$. Water–water impact results in jet breakup, but with much smaller droplets being ejected from the jet.

Collision dynamics are displayed in Fig. 5 for an impact $We = 123$ with pool depth of 25 mm. For water–water impact, a jet is formed. However, the jet breaks up into fewer droplets as opposed to the multiple droplet breakup observed at $We = 206$ at the same depth. Similar to $We = 206$, however, was the observation of droplets floating as witnessed at 105 ms after impact. Impact with the HFE7100 pool (Fig. 5) resulted in jet formation with

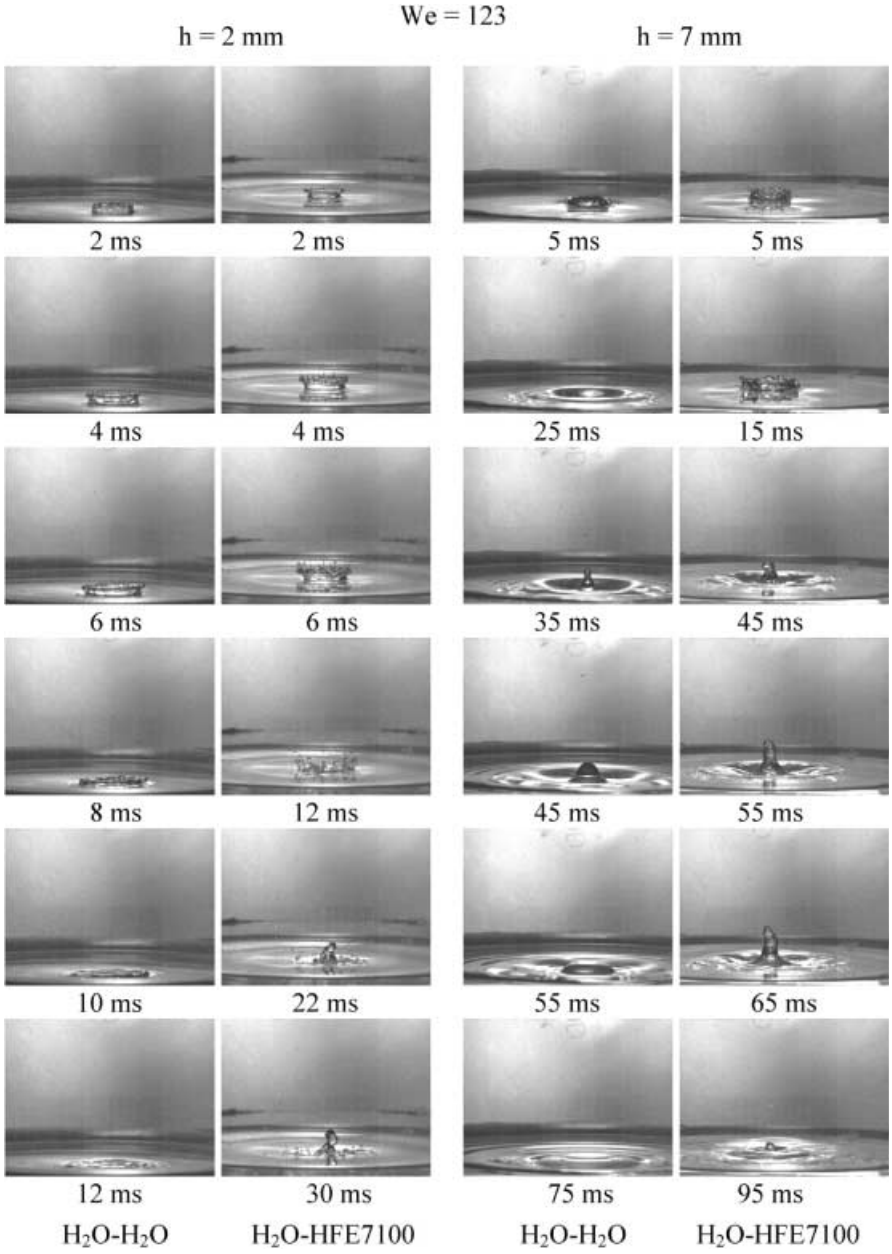

Fig. 4. Time-elapsed images of water droplet impingement upon a 2-mm and 7-mm liquid pool of water and HFE7100 for $We = 123$

no breakup, similar to water–HFE7100 impact for $We = 206$.

The formation of the secondary jet was only observed for water–HFE7100 impact. Secondary jet formation was first observed by Worthington (1908) for water–water impact for experiments in which the liquid column did not breakup. Rein (1993) suggested that the observation of secondary jet formation is similar to spreading and retraction for a spreading lamella for droplet impact on solid surfaces. Present observations were similar to Worthington's (1908) in that, for *We* equal to 123 and 206, water–water impact resulted in liquid column breakup and no secondary jet formation. However, water–HFE7100 impact resulted in secondary jet formation at $We = 206$. The absence of the secondary jet for lower *We* number suggests that secondary jet formation is dependent on the impact energy of the impinging droplet.

The separation of droplets from the jet is related to impact velocity (Rein 1993). Hallett and Christensen (1984) reported a critical impact ratio, $L = 7$ (defined as the ratio of kinetic energy to surface energy) when droplets were observed to separate from the jet for water droplet impact into a water pool 20 cm deep. They related L to the impact *We* number using the relation $L = We/3$. However, as pointed out by Rein (1993), explicit calculation of the ratio of kinetic energy to surface energy yields $L = We/12$. Thus, the critical impact *We* number reported by Hallett and Christensen (1984) for droplet separation from the jet is 84 (Rein 1993). At $We = 206$ and $We = 123$, impact of the water droplet upon the water surface resulted in jet formation and subsequent jet breakup. Water droplet impact with HFE7100 resulted in jet formation, yet under the same impact *We* number for water–water impact, the jet did not breakup. The critical impact *We* number for jet breakup was measured as a function of depth for

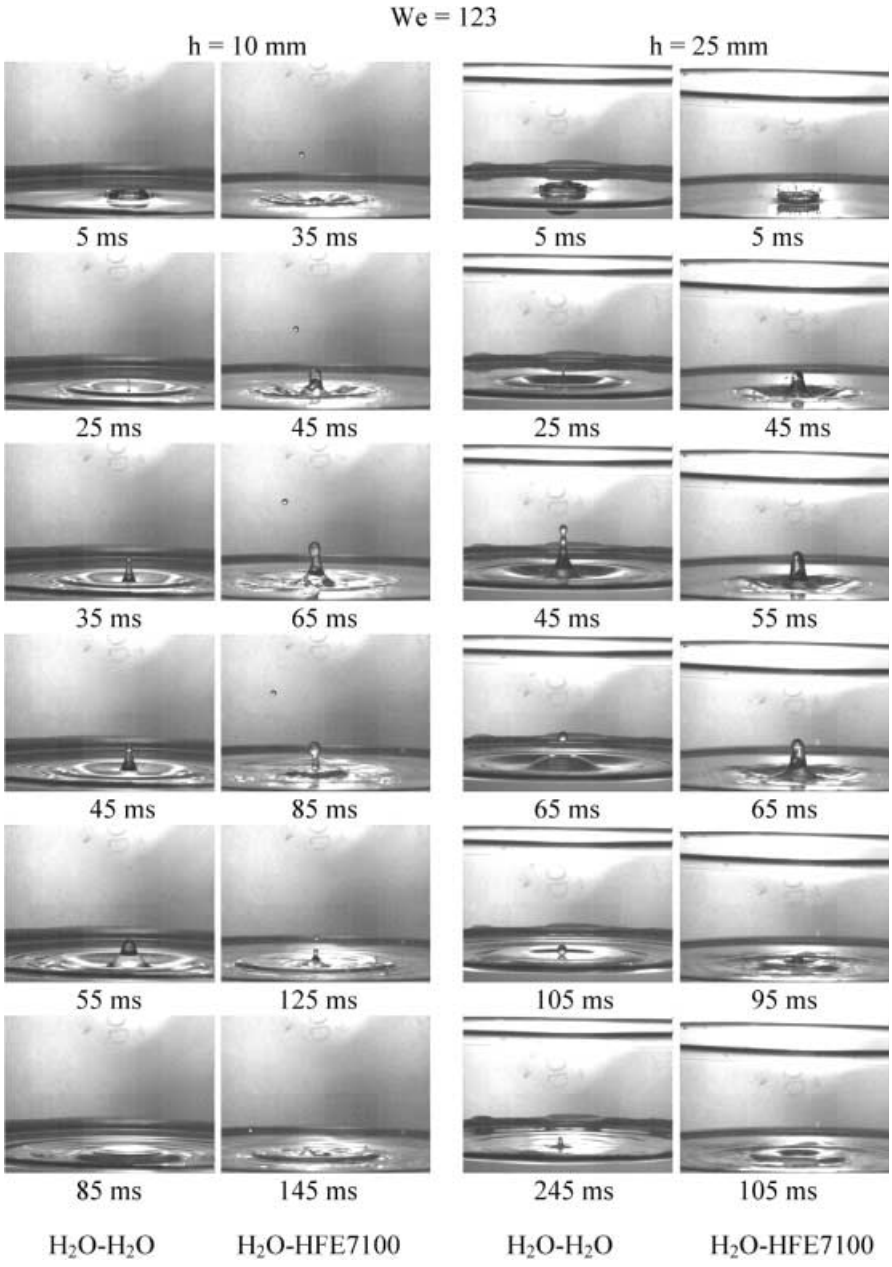

Fig. 5. Time-elapsed images of water droplet impingement upon a 10-mm and 25-mm liquid pool of water and HFE7100 for $We = 123$

Table 2. Summary of experimental observations

Depth (mm)	H_2O–H_2O				H_2O–HFE7100			
	$We = 5.5$	$We = 123$	$We = 206$	We_c	$We = 5.5$	$We = 123$	$We = 206$	We_c
2	NJ	NJ	NJ	NO	NJ	NJ	NJ	NO
4	NJ	J-NB	J-NB	NO	NJ	J-NB	J-NB	NO
7	NJ	J-B	J-B	66	NJ	J-NB	J-NB	NO
10	NJ	J-B	J-B	54	NJ	J-NB	J-NB	NO
15	NJ	J-B	J-B	65	NJ	J-NB	J-NB	NO
20	NJ	J-B	J-B	58	NJ	J-NB	J-NB	NO
25	NJ	J-B	J-B	71	NJ	J-NB	J-NB	NO

NJ, no jet; J-B, jet breakup; J-NB, jet no breakup; NO, not observed

water–water impact as is seen in Table 2. The relative combined standard uncertainty in determining the critical *We* number was ±8%. The critical *We* number remained relatively constant with increasing depth. It should be noted that the values reported here are lower than those reported by Hallett and Christensen (1984). However, the depth of the water pool used by Hallet and Christensen (1984) was 20 cm. This is eight times deeper than the deepest pool

considered in the present experiments – 25 mm. Therefore, direct comparison of critical impact *We* number with values measured by Hallett and Christensen (1984) is not justified.

A vast amount of literature is available regarding liquid jet breakup due to instability (Rayleigh 1882; Lin and Reitz 1998). These studies have focused on the breakup of a liquid jet comprising a single fluid emanating from a nozzle into a quiescent gas. Such analyses may be extrapolated to the present experiments with some assumptions. First, the jet that rises above the liquid surface is assumed to be similar to a jet emanating from a nozzle. Secondly, it must also be assumed that, in the case of water–HFE7100 impact, the jet comprises only HFE7100.

Reitz and Bracco (1986) have delineated jet breakup into four different regimes, Rayleigh regime, wind-induced regime, second wind regime, and the atomization regime. The Rayleigh and wind-induced breakup regime are characterized by a low-speed jet issuing from a nozzle. The second wind regime and atomization regime are known to occur for very high jet velocities. The different regimes can be characterized by estimating the jet and gas Weber number (Chigier and Reitz 1996). The velocity that appears in both Weber numbers is based on the relative velocity between the gas and the jet. However, measuring the gas velocity induced by the jet is difficult. Thus, characterizing the specific regime quantitatively is problematic.

The type of breakup observed in the present experiments is not characteristic of very high jet velocities (i.e., second wind and atomization regime). Rather, it is assumed that liquid jet breakup occurred within the Rayleigh breakup regime. Within the Rayleigh breakup regime, the size of the droplets pinched off from the jet are on the order of or larger than the jet diameter. Such behavior was observed in the present experiments. For the Rayleigh breakup regime, the breakup length of the jet scales linearly with the jet velocity (Lin and Reitz 1998). Thus, a jet with a given velocity must reach a certain length before droplets can be pinched off from the jet. The velocity of the jet issuing from the liquid pool was estimated from the images of the collision dynamics. At all depths where a jet is formed, the velocity of the jet rising from the HFE7100 pool is considerably lower than the jet rising from the water pool. For example, at a depth of 7 mm, the velocity of the water jet was measured to be 0.6 m/s, whereas the velocity of the HFE7100 jet was measured to be 0.2 m/s. Thus, the lower velocity of the HFE7100 jet suggests that the jet velocity is too low such that the jet does not reach the necessary breakup length.

Closer inspection of the liquid column for water–HFE7100 impact indicated that water droplets may be entrained within the jet of HFE7100. In order to investigate this supposition, a sequence of experiments was performed by dying the impacting water droplet green using a domestic food dye, to determine whether water droplets are entrained within the jet. Upon impact, the water droplet was observed to break up and indeed, water droplets were inside the jet. It is believed that the encapsulation of water droplets within the HFE7100 jet may act to reduce the jet velocity, precluding breakup. Therefore, no critical impact Weber number can be defined for water–HFE7100 impact over the range of velocities considered.

The liquid column height was measured for both water–water and water–HFE7100 impact. This height was defined as the height the liquid column rises above the free surface prior to jet breakup. Figure 6 displays the liquid column height above the free surface as a function of depth for water–water impact. The liquid column height was obtained by averaging the measurement over three consecutive runs for each depth. The error bars represent the standard deviation of three measurements at each height. At $We = 206$, the jet height reaches a maximum value at a depth of 7 mm. As the depth is increased to 10 mm, the maximum jet height decreases dramatically. Comparing this with a lower impact velocity and therefore lower impact *We* number, differences were observed. At $We = 123$, the liquid column height increases to a maximum at the 7-mm depth but a sharp decrease at the 10-mm depth, observed at $We = 206$, was not seen. In addition, the overall height is lower at $We = 123$ compared with $We = 206$. Hallett and Christensen (1984) have reported that the jet height is related to impact energy, thus lower impact energy results in a lower jet height. The reduction in jet height with a reduction in impact *We* is in qualitative agreement with their work.

The height of the liquid column was also measured for water–HFE7100 impact and is displayed in Fig. 7. For $We = 123$ and 206, the height of the liquid column increased and remained constant for depths above 15 mm. The height of the liquid column did not decrease dramatically beyond the 7-mm depth, as was observed in water–water impact at $We = 206$. A similarity to water–water impact was that the overall height is lower at $We = 123$ compared with $We = 206$. As discussed earlier, Macklin and Hobbs (1969) observed that the maximum jet height increased with increasing depth and subsequently decreased as the liquid pool depth was increased beyond 7 mm for water–water impact. The measurement of the liquid column height for water–water impact at $We = 206$ is in qualitative agreement with Macklin and Hobbs

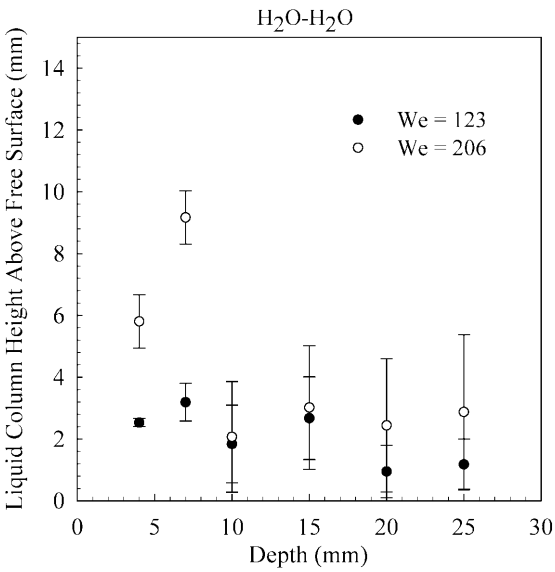

Fig. 6. Measured liquid column height above the free surface for water–water impact at $We = 123$ and $We = 206$

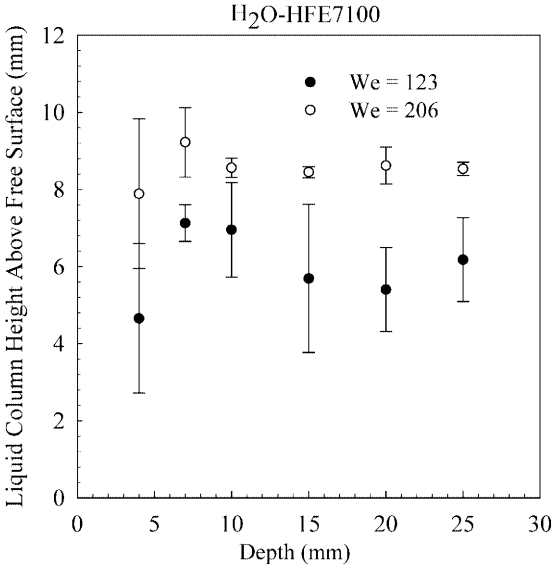

Fig. 7. Measured liquid column height above the free surface for water–HFE7100 impact at $We = 123$ and $We = 206$

(1969). Water–water impact at $We = 123$, however, resulted in little change in the liquid column height with increasing depth. For impact with HFE7100 at $We = 123$ and 206, the jet height first increases with liquid depth then remains nearly constant over the range of depths studied. Differences in the magnitude of liquid column height between water–water and water–HFE7100 impact are related to the inability of the liquid column to break up in the HFE7100 pool.

While impact at $We = 206$ and $We = 126$ remained within the splashing regime, attention will now be focused on the impact within the coalescing regime. Experiments were performed with the same initial droplet size as $We = 206$ and $We = 123$ but with an impact velocity of 0.36 m/s, resulting in an impact $We = 5.5$. Concurrent with previous investigations (Rodriquez and Mesler 1985; Hsaio et al. 1988; Rein 1996), the impacting water droplet was observed to coalesce with the liquid surface, i.e., no jet was observed to form. A summary of all the experimental observations is provided in Table 2.

4 Conclusions

An experimental study was performed for water droplet impingement on a liquid surface. The target surface consisted of two fluids, namely water and HFE7100, and the impact Weber number was varied from 5.5 to 206. The depth of the water and HFE7100 pool was varied from 2 mm to 25 mm. The collision dynamics of water in the HFE7100 pool was observed to be drastically different from that observed for the water droplet impingement on a water pool. The critical impact Weber number for jet breakup was found to be independent of liquid depth. Water–HFE7100 impact resulted in no jet breakup over the range of velocities studied, thus no critical impact Weber number can be defined for water–HFE7100 impact.

References

Al-Durrah MN, Bradford JM (1982) Parameters for describing soil detachment due to single waterdrop impact. Soil Sci Soc Am J 46:836–840

Avedisian CT, Koplik J (1987) Leidenfrost boiling of methanol droplets on hot porous/ceramic surfaces. Int J Heat Mass Transfer 30:1587–1603

Aziz S, Chandra S (2000) Impact, recoil and splashing of molten metal droplets. Int J Heat Mass Transfer 43: 2841–2857

Bola R, Chandra S (1999) Parameters controlling solidification of molten wax droplets falling on a solid surface. J Mater Sci 19:4883–4894

Bowden FP, Field JE (1964) The brittle fracture of solids by liquid impact, by solid impact, and by shock. Proc R Soc London A 282:331–352

Cai YK (1989) Phenomena of a liquid drop falling to a liquid surface. Exp Fluids 7:388–394

Chandra S, Avedisian CT (1991) On the collision of a droplet on a solid surface. Proc R Soc London A 432:13–41

Chandra S, Avedisian CT (1992) Observations of droplet impingement on a ceramic porous surface. Int J Heat Mass Transfer 35:2377–2388

Chigier H, Reitz RD (1996) Regimes of jet breakup and breakup mechanisms. In: Recent advances in spray combustion: spray atomization and drop burning phenomena. Reston, New York

Edgerton HE, Killian JR (1939) Flash! Seeing the unseen by ultra high speed photography. Hale, Cushman and Flint, Boston

Engel OG (1955) Waterdrop collisions with solid surfaces. J Res Nat Bur Stand 5:281–298

Hallett J, Christensen L (1984) Splash and penetration of drops in water. J Rech Atmos 18:225–242

Hsiao M, Lichter S, Quintero LG (1988) The critical Weber number for vortex and jet formation for drops impinging on a liquid pool. Phys Fluids 31:3560–3562

Jayaratne OW, Mason BJ (1964) The coalescence and bouncing of water drops at an air/water interface. Proc R Soc London A 280:545–565

Kang BS, Lee DH (2000) On the dynamic behavior of a liquid droplet impacting upon a inclined heated surface. Exp Fluids 29:380–387

Ko YS, Chung SH (1996) An experiment on the breakup of impinging droplets on a hot surface. Exp Fluids 21:118–123

Lesser MB (1981) Analytical solutions of liquid-drop impact problems. Proc R Soc London A 377:289–308

Levin Z, Hobbs PV (1971) Splashing of water drops on solid and wetted surfaces: hydrodynamics and charge separation. Phil Trans R Soc London A 269:555–585

Lin SP, Reitz RD (1998) Drop and spray formation from a liquid jet. Annu Rev Fluid Mech 30:85–105

Macklin WC, Hobbs PV (1969) Subsurface phenomena and the splashing of drops on shallow layers. Science 166:107–108

Oliver JF (1984) Initial stages of ink jet drop impaction, spreading and wetting on paper. Tappi J 67:91–94

Pumphrey HC, Crum LA, Bjørnø L (1989) Underwater sound produced by individual drop impacts and rainfall. J Acoust Soc Am 85:1518–1526

Rayleigh JWS (1882) Further observations upon liquid jets, in continuation of those recorded in the Royal Society's Proceedings for March and May, 1879. Proc R Soc London 34:130–145

Rein MJ (1993) Phenomena of liquid droplet impact. Fluid Dyn Res 12:61–93

Rein MJ (1996) The transition regime between coalescing and splashing drops. J Fluid Mech 306:145–165

Reitz RD, Bracco FV (1986) Mechanisms of breakup of round liquid jets. In: The encyclopedia of fluid mechanics. Gulf, Houston

Reynolds O (1875) On the action of rain to calm the sea. Proc Manchester Lit Philos Soc 14

Reynolds O (1881) On the floating of drops on the surface of water depending only on the purity of the surface. Proc Manchester Lit Philos Soc 21
Rodriguez F, Mesler RJ (1985) Some drops don't splash. J Colloid Interface Sci 106:347–352
Rodriguez F, Mesler RJ (1988) The penetration of drop-formed vortex rings into pools of liquid. J Colloid Interface Sci 121:121–129
Schotland RM (1960) Experimental results relating to the coalescence of water drops with water surfaces. Discuss Faraday Soc 30:72–77
Shin J, McMahon TA (1990) The tuning of a splash. Phys Fluids A 2:1312–1316
Thompson JJ, Newall HF (1885) On the formation of vortex rings by drops falling into liquids, and some applied phenomena. Proc R Soc London 39:417–436
Wang AB, Chen CC (2000) Splashing impact of a single drop onto very thin liquid films. Phys Fluids 12:2155–2158
Worthington AM (1908) A study of splashes. Longmans, Green
Zhbankova SL, Kolpakov AV (1990) Collision of water drops with a plane water surface. Fluid Dynamics 25:470–473